Bordes, MC.; Vicent, M.; Moreno, A.; Moreno, R.; Borrell Tomás, MA.; Salvador Moya, MD.; Sanchez, E. (2013). Microstructure and photocatalytic activity of APS coatings obtained from different TiO2 nanopowders. Surface and Coatings Technology. 220:179-186. doi:10.1016/j.surfcoat.2012.08.059.

MICROSTRUCTURE AND PHOTOCATALYTIC ACTIVITY OF APS COATINGS OBTAINED FROM DIFFERENT TiO_2 NANOPOWDERS

M.C. Bordes[1], M. Vicent[1], A. Moreno[1], R. Moreno[2], A. Borrell[3], M.D. Salvador[3], E. Sánchez[1]

(1) Instituto de Tecnología Cerámica (ITC). Universitat Jaume I. Castellón, Spain.

(2) Instituto de Cerámica y Vidrio (ICV). CSIC. Madrid, Spain.

(3)Instituto de Tecnología de Materiales (ITM). Universidad Politécnica de Valencia. Valencia, Spain.

Abstract

In recent years, intense research has shown that thermal spray techniques, especially atmospheric plasma spraying (APS), can be used to obtain nanostructured TiO_2 coatings with effective photocatalytic activity.

This study compares the photocatalytic activity of APS coatings obtained from different powders: two nanostructured TiO_2 powders produced by spray-drying of two TiO_2 nanosuspensions with different solids contents, one spray-dried powder obtained from a suspension comprising a mixture of submicronic and nanometric TiO_2 particles and finally one commercial, nanostructured, TiO_2 spray-dried powder. All powders were characterised by XRD, FEG-ESEM, granule size distribution, and a flowability evaluation. Feedstock powders were then deposited on austenitic stainless steel coupons using APS. Hydrogen or helium was used as secondary plasma gas. Coating microstructure and phase composition were characterised using FEG-ESEM and XRD techniques; coating anatase content was quantified by the Rietveld method.

A significant amount of anatase to rutile transformation was found to take place during the plasma spraying process. In general, the coatings had a bimodal microstructure characterised

by the presence of completely fused areas in addition to non-molten areas consisting of agglomerates of anatase nanoparticles. Results also showed that anatase content and porosity of the coatings largely depend on the secondary plasma gas nature, as well as on the characteristics of the feedstock.

Finally the photocatalytic activity of the coatings was determined by measuring the degradation of methylene blue dye in an aqueous solution. A reasonably good fit of a first-order kinetic model to the experimental data was found for all coatings. The values of the kinetic constant were related to feedstock characteristics as well as to plasma spraying conditions.

1. INTRODUCTION

Coatings with photocatalytic properties have a series of functionalities of wide interest and applicability such as: self-cleaning effect or cleanability, anti-fogging effect, sterilising effect and air purification. Although there are many photocatalysts, TiO_2 is known to be the best material in terms of its chemical stability, low cost and lack of toxicity [1].

In the last few years intensive research has shown that thermal spray techniques, especially atmospheric plasma spraying (APS), high velocity oxy-fuel spraying (HVOF), and more recently suspension plasma spraying (SPS) can be used to obtain TiO_2 coatings with effective photocatalytic activity [2-4]. Although the inherent advantages of feeding nanoparticle suspension into the plasma torch instead of nanostructured powders has increased the interest for the preparation of nanostructured coatings by SPS [4,5], this technology also presents limitations when compared with more traditional powder-feeding methods. Although concentration of feeding suspensions in SPS technology has significantly increased in last years [6] this technology generally uses low concentration suspensions (< 10 vol.%) due to the problems of viscosity and operability of the atomizer or injector which feeds the suspension into the plasma torch. This implies, among other things, that a source as energetic

as the plasma is used for the evaporation of large quantities of solvent, leading to an inefficient energy consumption process. On the other hand, obtaining nanostructured coatings by APS requires the reconstitution of starting nanopowders into a sprayable size, since nanoparticles can not be deposited directly because of their low mass and their poor flowability. The main method to reconstitute the nanoparticles is the spray-drying route [7]. This method involves a previous preparation of the powder from suspensions. Since, a priori, limitation does not exist in the characteristics of the starting suspension, the solids content can be maximized, leading to a higher efficiency process in terms of energy consumption. In fact, a recent study based on life cycle assessment (LCA) methodology has shown that APS had a lower impact than that of the liquid feedstock plasma spraying processes [8]. More importantly, the previous powder preparation process associated with APS technique enables the design of feedstocks in which the characteristics of the agglomerated granules, such as density, primary particle size distribution inside the agglomerate as well as agglomerate size distribution can be conveniently adjusted. This variety in feedstock characteristics can be of great interest when designing the microstructure and final properties of coatings as set out elsewhere [9].

A key issue through all this research has been to preserve as high amount as possible of anatase phase in the coating due to its superior photocatalytical behaviour in comparison with rutile. In fact, many studies have shown the need to achieve a minimum amount of anatase phase in the coating to have some photocatalytic activity [10-12]. However controversy still remains with regard to the factors that control the TiO_2 phase distribution (anatase versus rutile) in the final layers. A mixture of anatase and rutile is always encountered regardless the nature and composition of the feedstock while the amount of these phases can widely vary [9,13,14]. Several spraying parameters, such as plasma arc current, the addition of secondary gas, the total plasma gas flow rate, or the ratio between the plasma power and the primary gas flow rate have to be very carefully adjusted in order to minimize the particle heat input [14].

Many authors have observed that the anatase content in the coatings strongly depends on the thermal spray process conditions [9,12,13,15]. Nevertheless, though in general the role of the feedstock on the final characteristics of the coating is clearly recognized, this aspect has been scarcely approached in the literature on APS TiO_2 coatings. Bertrand et al. [9] showed that the combination of low energy spraying conditions and dense powder with large agglomerate size produces coatings with very high anatase ratio. In another work Berger-Keller et al. [15] achieved high amount of anatase phase by using a spray-dried feedstock which had previously been obtained from a flocculated suspension which gave rise to dense, solid agglomerates. These authors state that the microstructure and properties of plasma sprayed TiO_2 coatings not only depend on various process parameters but also are markedly influenced by the characteristics of the feedstock. However, in this foregoing research the photocatalytic activity has not been addressed.

In this respect this work aims at preparing TiO_2 photocatalytic coatings by APS from nanostructured powders with different characteristics. Two nanostructured TiO_2 powders will be produced by spray-drying of two nanosuspensions with different solids contents, and another one will be spray-dried from a suspension comprising a mixture of submicronic and nanometric TiO_2 particles. With these three feedstocks, the impact of the solids content and particle size distribution of the starting suspension on the feeding powder characteristics and, then, on the final microstructure and photocatalytic activity of the resulting coatings will be assessed. For this purpose, a key plasma spraying condition such as the nature of the secondary gas (H_2 or He) will be varied.

2. EXPERIMENTAL PROCEDURE

2.1. Feed powder preparation and characterisation

One commercial nanopowder suspension of titania (AERODISP® W740X) and one nanopowder of titania (AEROXIDE® P25, respectively) were used. This powder contains

anatase and rutile phases in a ratio of about 3:1 [16]. The solids content of the commercial suspension was 10 vol.%. According to the supplier (DEGUSSA/EVONIK, Germany), the solid contained in the nanoparticle suspension was the same as that of the nanopowder solid sample. TEM micrographs (H7100, Hitachi, Japan) of the solid in this sample confirmed its nanometric size: ~ 20-40 nm [17]. In addition, a submicron-sized, high purity anatase (Merck, Germany) with a mean particle size of 0.35 μm and a specific surface area of 9.5 m^2/g was also used. Finally, a nanostructured, titania spray-dried commercial feedstock, TNN (NEOXID T101 nano, Millidyne, Finland) was used for comparison purposes (hereinafter nNN powder). Previous characterisation of this feedstock gave rise to the following data: primary particle size of 15-50 nm, specific surface area of 43 m^2/g and an approximate crystalline phase ratio anatase:rutile of 4:1.

The as-received, 10 vol.% TiO_2 suspension was referenced nD ("nano-diluted"). Well-dispersed TiO_2 nanoparticle suspension with high solids content (30 vol.%) was then obtained by dispersing the nanopowder (P25) in the nD suspension using a polyacrylic dispersant (DURAMAX™ D-3005, Rohm&Haas, USA), with 35 wt% active matter (PAA). The procedure followed to obtain this highly concentrated TiO_2 suspension has been set out elsewhere [18]. This 30 vol.% solids content suspension was referenced nC ("nano-concentrated"). On the other hand, a 30 vol.% suspension made up of 50 wt% of nanosized powder (P25) and 50 wt% of submicron-sized powder along with the required amount of the polyacrylic dispersant was prepared. The suspension was prepared by adding first the PAA required to disperse the nanosized titania (4 wt% with regard to nanoparticles) and then, the PAA required to disperse the submicronic powder (0.3 wt% with regard to submicron-sized particles). In a second step, nanosized and submicron-sized powder titania were added and the mixture was prepared under mechanical agitation and with sonication probe (1 min.). Given PAA contents refer to the active matter concentration. This last suspension was named snC ("submicronic-nanometric concentrated"). The procedure followed to obtain this highly

concentrated submicronic-nanometric TiO_2 suspension has also been previously reported for alumina-titania suspensions [19].

Spray-dried granules were obtained from the nD, nC and nsC suspensions in a spray dryer (Mobile Minor, Gea Niro, Denmark) with a drying capacity of 7 kg water/h. From these three suspensions the corresponding three spray-dried powders were then obtained (hereinafter referred as nD, nC and nsC powders). Granule size distribution was measured by laser light scattering (Mastersizer S, Malvern, UK). Agglomerate bulk density was calculated from powder tapped density by assuming a theoretical packing factor of 0.6, which is characteristic of monosize, spherical particles [20]. Powder flowability was evaluated in terms of the Hausner ratio, determined by dividing tapped density by bulk density. Free-flowing powders have a Hausner ratio < 1.25.

A field-emission environmental scanning electron microscope, FEG-ESEM (QUANTA 200FEG, FEI Company, USA) equipped with an energy-dispersive X-ray spectrometer (EDAX Genesis, USA) was used to analyse the feedstock microstructure.

2.2. Preparation and characterisation of coatings

TiO_2 coatings were deposited by APS on metallic substrates (AISI 304) prepared as set out elsewhere [21]. The plasma spray system consisted of a gun (F4-MB, Sulzer Metco, Germany) operated by a robot (IRB 1400, ABB, Switzerland). The deposition was made using argon as primary gas and, hydrogen or helium as secondary gas. Helium gas was used to reduce the heat intensity of the plasma jet. The main spraying conditions are set out in table I. An estimate of plasma enthalpy as reported elsewhere [22] is also included in this table. In addition, the following spraying conditions were kept constant throughout all the experiments: Anode nozzle internal diameter = 6 mm, powder injector diameter = 2 mm, feedstock feed rate = 30 g/min and scanning step = 4 mm.

Coating crystalline phase compositions were evaluated by X-ray diffraction analysis (XRD). The XRD patterns were obtained using a Theta-Theta model diffractometer (D8 Advance,

Bruker, Germany) with CuKα radiation (λ = 1.54183 Å). The generator settings were 45 kV and 30 mA. The XRD data were collected in a 2θ of 5-90º with a step width of 0.015º and a counting time of 1.2 s/step by means of a VÅNTEC-1 detector. A quantitative phase analysis was conducted and the collected data were used in a Rietveld refinement [23,24]. In this study the 4.2 version of the Rietveld analysis program DIFFRACplus TOPAS was used, assuming a pseudo-Voight function to describe peak shapes. The refinement protocol included the background, the scale factors and the global-instrument, lattice, profile and texture parameters. The basic approach consists in identifying first all the crystalline phases present in the sample and then inputting the corresponding basic structural data. Finally, computer modelling is used to find the best fit to experimental patterns. Content (wt%) and crystallite size of crystalline phases (anatase and rutile) were then calculated by this method. Rwp (R-weighted pattern) and GOF (Goodness Of Fit) parameters were calculated in order to evaluate the accuracy of results.

Roughness measurements were carried out by means of a contact profilometer HOMMELWERKE T8000 (HOMMELWERKE), using a 5-micron diamond cantilever with a 90º curvature. The roughness test consisted of obtaining 81 profiles of 4.8-milimeter length until obtaining a topographic map of 4.8x4.8mm. The cut-off used in order to obtain the roughness parameter (Ra) after the measurements was 0.8 mm.

A SEM instrument (JSM6300, JEOL, Japan) was also used to study the microstructure of the coatings. Finally, coating porosity and semi-molten particle fractions were measured on cross-sectional coating areas by image analysis (Image pro-Plus, Media Cybernetics, Inc., USA) of the micrographs obtained by an optical microscope (Microphot FX, Nikon, Japan) at 400 magnifications. The resolution was 0.1 μm. An average of 10 images, randomly located across the sample, were analysed for each sample in order to obtain a representative, complete scan of the whole cross-sectional area [7].

2.3. Photocatalytic activity determination in the coatings

The photocatalytic activity of the coatings was determined by studying the decomposition of methylene blue (MB) in aqueous solution. This study determined the variation of the MB concentration in a 5 ppm MB solution in contact with the photocatalytic coating, under UV radiation. The detailed description of the procedure has been recently reported [25]. In order to allow the MB to be adsorbed on to the TiO_2 surface, the test pieces were kept in contact with the solution for 24 h in the dark. During this time, MB concentration decreased less than 10 % of initial concentration. In addition, the dark test showed that MB concentration hardly varied after 30 min contact between the MB solution and the coating. For this reason, the test pieces were kept in contact with the MB solution for 30 minutes in the dark, prior to irradiation, after which the MB concentration was determined. Finally, a blank, uncoated sample was tested in order to evaluate the influence of UV radiation on the decrease of MB concentration by photolysis.

3. RESULTS AND DISCUSSION

3.1. Spray-dried powder feedstock characterisation

A detailed characterisation of the powders obtained from the diluted and concentrated suspensions (nD and nC samples respectively) was reported in a previous work [18]. Thus, appropriate references will be done when necessary throughout the following sections.

Figure 1 shows FEG-ESEM micrographs at two magnifications of the commercial powder and the spray-dried powder obtained from the submicron and nanometric-sized mixture (nNN and nsC samples). As it can be seen most granules exhibit the typical spherical or doughnut-shape morphology of spray-dried agglomerates [26]. The same was observed for nD and nC powders [18]. In addition, good homogeneity (round morphology) is also observed in the agglomerates of these two powders (nNN and nsC samples) meanwhile the commercial nNN sample displays a wider granule size distribution containing finer granules than those of the

nsC sample. Higher magnification observation of the solid areas of the agglomerated powders (Figure 1) reveals that the granules are porous and formed by the agglomeration of individual nanoparticles. As expected the presence of submicron-sized particles is clearly visible in the nsC sample, but also in the nNN sample, which apparently should only be made up of nanometric particles.

Granule size distribution, measured by laser light scattering, is summarised in table II where three typical average undersize granule diameters (D_{10}, D_{50} and D_{90}) are shown. All the powders exhibit similar, quite narrow granule size distributions except nNN sample whose distribution shifts to smaller granule sizes. This demonstrates that the prepared suspensions are quite homogeneous even in the case of nsC sample where nano and submicron-sized particles are randomly distributed. With regard to nNN powder, this sample shows a distribution with a significant content of small agglomerates whose size is lower than 10 μm. The presence of so small granules can negatively affect the powder feeding operation into the plasma torch due to the poor flowability of fine agglomerates [26]. It is generally recognized that thermal spray powders exhibit agglomerate size distributions ranging from 10 to 150 μm [27].

Table II also lists two other properties of interest for spray-dried powders to be used as feedstock in plasma spraying: the Hausner ratio, which is related to the flowability of the powder and the agglomerate bulk density, which is directly related to its weight. According to literature [27,28], relatively dense (higher than 1000 kg/m^3 apparent density) and free-flowing agglomerates are necessary for a suitable feeding into the plasma torch. In general, all the samples exhibit adequate characteristics to be used as APS powders. However, significant differences can be again observed among the four samples. With regard to the agglomerate bulk density, sample nsC shows the highest value as a consequence of the better packing efficiency inside the agglomerate associated with the submicronic-nanometric particle arrangement. In addition, the agglomerate density of the other two powders obtained in this

research (nD and nC samples) is much higher than that of the nNN sample. Although no information about the preparation of the commercial powder is available, the high density of nD and nC samples is related to the good dispersion state of the corresponding nD and nC suspensions used to spray-dry these powders [18]. Regarding the flowability of the samples, powders nC and nsC show the lowest Hausner ratios (better flowability) mainly due to the optimum combination of large agglomerate average size and round morphology of the granules. On contrary, samples nNN and nD exhibit higher Hausner ratios (poorer flowability) than those of the other two powders as a consequence of a smaller average agglomerate size and the presence of less spherical (deformed) agglomerates respectively as set out in the previous research [18].

3.2 Microstructure and phase distribution of the coatings

Eight different types of coatings were obtained from the four spray-dried feedstocks (nNN, nD, nC and nsC) by depositing all powders in two different spraying conditions, using hydrogen or helium as plasma secondary gas (Table I). Figure 2 shows SEM micrographs of these four coatings. As no significant differences were observed between the micrographs of the different coatings, and for the sake of simplicity, only the micrographs corresponding to samples obtained with He are set out. Besides, higher magnification micrographs for nD and nC coatings are shown in reference [18]. The coatings displayed the typical microstructure of TiO_2 coatings deposited from nanostructured feedstock [15,18,29,30]. The literature indicates that such coating microstructures basically comprise two clearly differentiated zones, yielding a bimodal structure. Thus one coating region, which is completely melted (marked M in figure 2), mainly consisted of an amorphous titania matrix with recrystallised nanometre-sized grains of rutile. Rietveld analysis revealed that the rutile crystallite size in the coatings ranged from 46 nm (coating nsC obtained in H_2) to 108 nm (nNN coating obtained in helium). The other coating region, which is only partially melted (marked PM), largely retained the microstructure of a slightly sintered or non-sintered starting powder. This microstructure was

therefore principally made up of nanometre to submicron-sized grains of anatase. Finally with regard to the porosity, all the coatings were porous, exhibiting the typical lamellar structure of plasma sprayed coatings. Thus smaller pores are located within individual lamellae and larger pores are found along the interlamellar boundaries, as seen in the micrographs (Figure 2 and reference [18]).

In view of the above, the total porosity of the coatings, as well as the amount of semi-molten areas, was estimated by image analysis at 400 magnifications. These magnifications enable porosity and semi-molten areas to be estimated for comparative purposes. However, pores cannot be readily distinguished from semi-molten areas because both issues are detected as black particles. To perform this identification, the binarised image of the sample is first obtained in black and white colours following a procedure set out elsewhere [7]. The porosity and semi-molten areas results for all coatings are represented as histogram plots in figure 3. As it can be seen in figure 3 (left), the porosity of all the coatings presents values typically found in APS coatings. In general, porosity increases when helium gas is used as a consequence of the lower plasma heat input as reported elsewhere [12,15,30]. However, the impact of the characteristics of the feedstock on the coating porosity was not very significant. This is probably because the calculation of porosity by image analysis underestimates the contribution of the finest pores contained in the non-melted powder agglomerates incorporated in the matrix as reported in the literature [9]. For this reason, the effect of the intragranular porosity of the feedstock agglomerates is not easily observed. Regarding the unmelted or partially melted areas, as expected the use of helium as plasma gas leads to a strong increase in these areas. Again a lower plasma heat input provided by the use of helium instead of hydrogen is the reason for this finding. More importantly the amount of semi-molten areas in the coating obtained from the nsC powder in helium is the highest as a consequence of the characteristics of the agglomerates comprising this powder. These findings confirm the previous results set out in the literature by Bertrand et al. [9] about TiO_2

coatings obtained from spray-dried powders containing granules of different morphologies and sizes. These authors evidenced that to increase the partially molten regions which are made up of anatase phase, the feedstock has to contain dense and large (higher than 90 μm size) granules, and the plasma heat input has to be low. This is because only the outer surface of the granule is fully melted whereas in the inner part the particle packing remains very similar to the initial one. Additionally, the presence of submicron-sized particles in the feedstock agglomerates can also contribute to the increase of these unmelted and scarcely sintered areas.

Roghness measurements (Ra parameter) of all the coatings were determined. Small differences between the coatings were observed. The Ra values ranged from 3.5 ± 0.3 μm to 5.7 ± 0.4 μm. No correlation between nanometric or submicrometric character of the primary particles comprising the spray-dry feedstock and coating roughness was found. For the sake of example, top-surface micrographs of nC-He coating (Ra = 4.9 ± 0.4 μm) and nD-He coating (3.8 ± 0.2 μm) have also been included in figure 2.

The XRD patterns of the coatings were also obtained. In all the cases the coatings were mainly made up of rutile and anatase with minor amounts of Magneli phases as reported elsewhere [31]. Figure 4 shows an example of these patterns given by the nsC coating obtained in hydrogen and helium.

The rutile and anatase content in the coatings were calculated by the Rietveld method as explained above. The major crystalline phase was rutile; the rutile content ranged from 18 to 60 wt%. However for photocatalytic application, anatase is the most important phase. Figure 5 represents the calculated anatase content of all the coatings. On the top of each histogram the anatase crystallite size (in nm) calculated by Rietveld is also detailed. As reported in the literature [12,30] coatings obtained with helium result in much higher amount of anatase phase regardless the feedstock used. Concerning the influence of the starting powder, the nsC feedstock gave rise to the highest amount of anatase due to the higher presence of unmolten

areas according to figure 3 (right). These findings are in good agreement with the results reported in the literature. In this respect, most of the research on TiO_2 APS coatings demonstrates that the metastable anatase phase in these coatings is almost exclusively associated with the presence of non-melted starting agglomerates. In fact, some authors [9] have proved a good linear fit between the areas of the partially molten zones in the coating with the anatase content. Nevertheless, although some other authors [32] have showed that some anatase is encountered even when the powder feedstock is purely rutile, the content of anatase achieved in the coating is always lower than that obtained starting from anatase powder. In the present work, a relatively low amount of anatase content has been obtained in the coatings as shown in figure 5. However when plotting the anatase content in the coatings versus the amount of non-molten areas (Figure 6), despite the data scattering observed the finding appears to indicate that the preserved anatase particles in the non-molten areas is the most relevant contribution to the anatase content in the coating. This statement is probably reinforced by the fact that all the plasma spray parameters (except the secondary plasma gas) which can influence the anatase/rutile transition were kept constant throughout the experiments.

Finally, as regards the crystallite size, an increase of anatase crystallite size is observed in all the coatings when using H_2 instead of He as secondary gas. In fact, when hydrogen is used the heat transfer from the plasma to the feed material is enhanced. As a consequence the particles reach more elevated temperature leading to a higher sintering effect. Moreover the crystallite size in the coatings obtained from exclusively nanostructured powders (samples nNN, nD and nC) in helium shows a good agreement with the nanoparticle size determined for the nanopowders comprising these three feedstock as set out above. However the effect of the plasma gas on the anatase crystallite size of the coating obtained from the submicronic-nanometric feedstock (sample nsC) is much less evident. In this case, the anatase crystallites forming the submicronic particles are less influenced by the energetic conditions of the

plasma gas, probably because these nano-crystallites are more clustered in the submicron-sized particle arrangement leading to decreased effective anatase sinterability.

3.3 Photocatalytic activity of the coatings

The photocatalytic activity of the coatings was determined by measuring the degradation of Methylene Blue (MB) dye in an aqueous solution. Figure 7 shows the variation in MB with irradiation time for the solutions in contact with nsC (helium) coating and with a blank substrate.

Clear differences were found in the concentrations in the solutions, at each irradiation time. A pronounced decrease in concentration is observed for the coated sample whereas blank substrate shows no significant degradation after the UV irradiation. This finding confirms the photocatalytic activity of the tested coating. Similar results were obtained for all the coatings, independently of the feedstock used.

The variation in MB concentration with time may be represented using a first-order kinetic equation as previously reported by some of the authors [25]. The constant of photocatalytic activity k (h^{-1}) can be then calculated from the kinetic equation fit. A higher value of k means faster degradation rate of the organic molecule of MB, that is, a higher photocatalytic activity. Rate constants determined from the kinetic model for all coatings are shown in figure 8. In all the cases the correlation coefficients were higher than 0.987 indicating a reasonably good fit of the kinetic model to experimental data. Similar fit was found by some of the authors in the aforementioned previous research [25] with SPS titania coatings, although the values of the constant rates were higher than those observed when using powders as feedstocks.

With the aim to evaluating the magnitude of the photocatalytic effect of these coatings, figure 8 also shows the photocatalytic activity of a sol-gel, TiO_2 commercial photocatalytic coating (Nano-X GmbH, Germany). This coating was applied following the instructions given by the supplier (spraying of the dispersion on the substrate surface and subsequent thermal treatment at 400 ºC). The coating is obtained by spraying two water-based dispersions: an under layer or

primer named x-clean® PK 3033 P (SiO_2-nanocomposite) and a top or functional layer named x-clean® PK 3033 F (modified nano-titanium oxide). The final top layer was characterised giving rise to the following information: 350 ± 10 nm thickness, Ra = 1.0 ± 0.1 μm and a microstructure comprising anatase nanocrystals of approximately 40-50 nm size. The FEG-ESEM micrograph of this coating is shown in figure 9 confirming the nanostructured character of the coating. This reference coating was also used in a previous research [25].

As it can be seen, in general, the photocatalytic effect of the APS coatings obtained in this work shows similar values to that of the commercial coating. As expected, for all the feedstocks, the coatings obtained with He display higher photocatalytic activity than those obtained with H_2 as a consequence of the increased amount of preserved anatase phase as set out above. More interestingly the maximum photocatalytic activity was found for the nsC coating which in turn contained the maximum amount of anatase phase. Thus the feedstock obtained by combining nanometric and submicronic particles in the micrometric agglomerates gave rise to coatings with the best photocatalytic performance. This result is of particular relevance since, as set out above, the combination of nanometric-submicronic particles makes the suspension preparation easier (higher solids content with lower viscosity suspensions can be obtained) resulting in highly homogenous, dense and free-flowing spray-dried feedstocks with excellent properties to be plasma sprayed.

Figure 10 plots the value of k versus anatase content of all the obtained coatings. For the sake of comparison the value of the k constant for the blank sample exclusively associated with a photolysis effect (there is not photocatalytic activity) is also included. As it can be seen, although the data show significant scattering, the photocatalytic activity of the coatings in the MB conversion correlates with the anatase phase content. This finding is consistent with most of previous research [13,29,30]. Hence, higher anatase phase content results in faster degradation of MB. As also previously reported [13] the anatase fraction was more dominant factor than the anatase crystallite size. This statement is confirmed by the fact that the coating

with the highest photocatalytic activity (sample nsC in helium) at the same time shows a higher crystallite size. In addition, figure 9 demonstrates the presence of an anatase content threshold for MB effective degradation. Hence for anatase content lower than 10 wt%, although the photocatalytic degradation is between 5-7 times faster than the photolysis effect (k constant values 5-7 times higher than that of the blank sample), the k value is almost constant throughout this anatase content range. However the k value significantly increases for anatase content exceeding this threshold. The presence of an anatase content threshold was previously reported in the literature [29] however the value of the threshold significantly differed from the value obtained here since the coatings and the photocatalytic test used were completely different.

On the other hand the lack of a correlation between photocatalytic activity and anatase content has also been reported in the literature. In a recent research by some of the authors [25] this unsuitable correlation was, in some extent, attributed to the fact that the amount of anatase phase determined by XRD does not suitably represent the amount of anatase phase onto the surface of the coating. The influence of others factors such as porosity or surface activity (hydroxylation or other adsorbed species) of the coating have been also reported but not scientifically proved [12,33]. In fact other authors have shown the photocatalytic activity of SPS titania coatings mainly made up of rutile [34]. These reasons together with the fact that the photocatalytic activity of TiO_2 APS coatings shows relatively good values make it necessary to carry out further research so as to clarify the contribution of other factors rather than the anatase phase content in the coating.

4. CONCLUSIONS

This study compares the microstructure and photocatalytic activity of APS coatings obtained from different powders: two nanostructured TiO_2 powders produced by spray drying of two TiO_2 nanosuspensions with different solids contents, one spray-dried powder obtained from a

suspension comprising a mixture of submicronic and nanometric TiO_2 particles and, finally, one commercial, nanostructured, TiO_2 spray-dried powder.

Despite the differences observed in the four powders studied, in general, all the samples exhibit adequate characteristics in terms of granule bulk density and powder flowability so as to be used as APS powders. In particular, the use of a suspension containing two particle size distributions (submicron- and nano-sized particles) leads to a spray-dried powder with the best density and flowability to be used as APS feedstock.

Moreover all coatings displayed a bimodal microstructure with partially molten agglomerates that retained the initial nanostructure of the feedstock surrounded by a fully molten matrix. In all the cases the coatings were mainly made up of rutile (18-60 wt%) and anatase (2.2-18 wt%). It has been shown that the preserved anatase particles in the non-molten areas are the most relevant contribution to the anatase content in the final coatings. As expected, coating porosity as well as partially molten areas proportion increase when helium is used instead of hydrogen as plasma secondary gas, as a consequence of the lower plasma heat input. However, the impact of the characteristics of the feedstock on the coating porosity was not so significant. On the contrary an increase in the anatase crystallite size is observed in all the coatings when using H_2 instead of He. This is a consequence of the higher sintering effect provided by the hydrogen plasma. The feedstock obtained from a mixture of submicronic and nanometric particles leads to higher amount of unmolten areas and consequently to higher content of anatase phase due to the characteristics of the agglomerates forming this feedstock (high density and large size) as well as to the reduced sinterability of the submicron-sized particles.

The photocatalytic activity of the coatings was determined by measuring the degradation of Methylene Blue (MB) dye in an aqueous solution. A reasonably good fit of a first-order kinetic model to experimental data was found for all the coatings. Values of the kinetic constant display a similar magnitude to that of a commercial sol-gel coating. Although a

direct correlation between anatase content and photocatalytic activity was found, the significant data scattering observed, along with the existence of an anatase content threshold for photocatalytic MB degradation indicate the contribution of other factors apart from the anatase content in the coatings. The coatings obtained from the submicronic-nanometric feedstock resulted in the best photocatalytic performance.

Acknowledgements

This work has been supported by the Spanish Ministry of Science and Innovation (projects MAT2009-14144-C03 and PID-600200-2009-5), and the Institute of Small and Medium-sized Enterprise (IMPIVA) of the Autonomous Government of Valencia through the European Social Fund (ESF) Operational Programme for the Valencia Region 2007-2013 and a Complementary Action (ACOMP/2009/221).

REFERENCES

1. M.A. Henderson. *Surf. Sci. Rep.* 66 (2011) 185-297.
2. Z. Yi, J. Li, W. Wei, J. Wang, S.W. Lee. *Ceram. Int.* 34 (2008) 351-357.
3. G. Bolelli, V. Cannillo, R. Gadow, A. Killinger, L. Lusvarghi, J. Rauch. *Surf. Coat. Technol.* 203 (2009) 1722-1732.
4. L. Pawlowski. *Surf. Coat. Technol.* 203 (2009) 2807-2829.
5. A. Killinger, R. Gadow, G. Mauer, A. Guinard, R. Vaβen, D. Stöver. *J. Therm. Spray Technol.* 20 (2011) 677-695.
6. P. Fauchais, G. Montavon, R.S. Lima, B.R. Marple. *J. Phys. D: Appl. Phys.* 44 093001 doi:10.1088/0022-3727/44/9/093001.
7. E. Sánchez, A. Moreno, M. Vicent, M.D. Salvador, V. Bonache, E. Klyatskina, I. Santacruz, R. Moreno. *Surf. Coat. Technol.* 205 (2010) 987-992.
8. A. Moign, A. Vardelle, N. J. Themelis, J. G. Legoux. *Surf. Coat. Technol.* 205 (2010) 668-673.
9. G. Bertrand, N. Berger-Keller, C. Meunier, C. Coddet. *Surf. Coat. Technol.* 200 (2006) 5013-5019.
10. F.L. Toma, D. Sokolov, G. Bertrand, D. Klein, C. Coddet, C. Meunier. *J. Therm. Spray Technol.* 15 (2006) 576-581.
11. N. Dejang, A. Watcharapasorn, S. Wirojupatump, P. Niranatlumpong, S. Jiansirisomboon. *Surf. Coat. Tech.* 204 (2010) 1651-1657.
12. F.L. Toma, N. Keller, G. Bertrand, D. Klein, C. Coddet. *Int. J. Photoener.* 5 (2003) 141-145.
13. Ch. Lee, H. Choi, Ch. Lee, H. Kim. *Surf. Coat. Tech.* 173 (2003) 192-200.
14. J.R. Colmenares-Angulo, V. Cannillo, L. Lusvarghi, A. Sola, S. Sampath. *J. Mater. Sci.* 44 (2009) 2276-2287.

15. N. Berger-Keller, G. Bertrand, C. Filiare, C. Meunier, C. Coddet. *Surf. Coat. Technol.* 168 (2003) 281-290.
16. T. Ohno, K. Sarukawa, K. Tokieda, M. Matsumura. *J. Catal.* 203 (2001) 182-186.
17. M. Vicent, E. Sánchez, I. Santacruz, R. Moreno. *J. Eur. Ceram. Soc.* 31 (2011) 1413-1419.
18. M. Vicent, E. Sánchez, A. Moreno, R. Moreno. *J. Eur. Ceram. Soc.* 32 (2012) 185-194.
19. T. Molina, M. Vicent, E. Sánchez, R. Moreno. *Mater. Res. Bull.* 47 (2012) 2469–2474.
20. J.L. Amorós, A. Blasco, J.E. Enrique, F. Negre. *Bol. Soc. Esp. Ceram. Vidr.* 26 (1987) 31-37.
21. E. Sánchez, V. Cantavella, E. Bannier, M.D. Salvador, E. Klyastkina, J. Morgiel, J.Grzonka, A. Boccaccini. *J. Therm. Spray Technol.* 17 (2008) 329-337.
22. C. Delbos, J. Fazilleau, V. Rat, J F. Coudert, P. Fauchais, B. Pateyron. *Plasma Chem. Plasma P.* 26 (2006) 371–391.
23. R. E. Young (Ed.). The Rietveld method. University press, Oxford, 1996.
24. H.M. Rietveld. *J. Appl. Crystal.* 2 (1969) 65-71.
25. E. Bannier, G. Darut, E. Sanchez, A. Denoirjean, M.C. Bordes, M.D. Salvador, E. Rayón, H. Ageorges. *Surf. Coat. Technol.* 206 (2011) 378-386.
26. F. Negre, E. Sánchez in: V.E. Henkes, G.Y. Onoda, W.M. Carty (Eds.). Science of Whitewares. American Ceramic Society, Ohio, 169-181, 1996.
27. X.Q. Cao, R. Vassen, S. Schwartz, W. Jungen, F. Tietz, D. Stöever. *J. Eur. Ceram. Soc.* 20 (2000) 2433-2439.
28. P. Fauchais, G. Montavon, G. Bertrand. *J. Therm. Spray Technol.* 19 (2010) 56-80.
29. F.L. Toma, L.M. Berger, D. Jaquet, D. Wicky, I. Villaluenga, Y.R. de Miguel, J.S. Lindeløv. *Surf. Coat. Technol.* 203 (2009) 2150-2156.
30. X.Y. Wang, Z. Liu, H. Liao, D. Klein, C. Coddet. *Thin Solid Films* 451-452 (2004) 37-42.
31. R.S. Lima, B.R. Marple. *Surf. Coat. Technol.* 200 (2006) 3428-3437.
32. H. Podlesak, L. Pawlowski, J. Laurenys, R. Jaworski, T. Lampke. *Surf. Coat. Technol.* 202 (2008) 3723-3731.
33. F.L. Toma, G. Bertrand, S. Begin, C. Meunier, O. Barrers, D. Klein, C. Coddet. *Appl. Catal. B-Environ.* 68 (2006) 74-84.
34. S. Kozerski, F.L. Toma, L. Pawlowski, B. Leupolt, L. Latka, L.M. Berger. *Surf. Coat. Technol.* 205 (2010) 980-986.

TABLES

Table I. Main plasma spraying parameters used in the experiments

Secondary plasma gas	Ar (slpm)	H_2 (slpm)	He (slpm)	$^{(1)}$I (A)	$^{(2)}$d (m)	$^{(3)}$v (m/s)	$^{(4)}\Delta$H (MJ/kg)
H_2	38	14	---	600	0.12	1	26 ± 2
He	40	---	20	600	0.12	1	12 ± 1

slpm = standard litre per minute, $^{(1)}$I = arc intensity, $^{(2)}$d = spraying distance, $^{(3)}$v = spraying velocity, $^{(4)}\Delta$H = enthalpy

Table II. Main powder characteristics of the four spray-dried feedstocks studied in this work

Feedstock characteristic	nNN	nD	nC	nSC
D_{10} (µm)	13	32	35	32
D_{50} (µm)	30	76	63	74
D_{90} (µm)	59	135	100	148
Granule bulk density (kg/m^3)	1250 ± 10	1870 ± 14	1630 ± 12	2080 ± 16
Hausner ratio	1.18 ± 0.04	1.20 ± 0.03	1.12 ± 0.03	1.11 ± 0.03

FIGURE CAPTIONS

Figure 1. FEG-ESEM micrographs at two magnifications of two studied spray-dried feedstock (nNN and nsC)

Figure 2. Cross section and two top-surface SEM micrographs of coatings obtained with He as secondary gas

Figure 3. Total porosity (left) and amount of semi-molten areas (right) for the coatings obtained from the four feedstock (nNN, nD, nC and nsC) with the two plasma gases (H_2 and He)

Figure 4. XRD pattern of the nsC coatings obtained with H_2 and He

Figure 5. Calculated anatase content (wt%) determined by XRD for the coatings obtained from the four feedstock (nNN, nD, nC and nsC) with the two plasma gases (H_2 and He). Anatase crystallite size (in nm) is shown on the top of each bar

Figure 6. Plot of anatase content (wt%) versus unmelted areas (%) evaluated from image analysis

Figure 7. Variation of MB concentration with UV irradiation time for solutions in contact with nsC (helium) coating and with a blank sample

Figure 8. Photocatalytic activity rate constants (k values) of all the coatings obtained. The k value of a sol-gel, commercial TiO_2 coating is also shown

Figure 9. Cross section of the commercial, sol-gel TiO_2 coating

Figure 10. Correlation between anatase content (wt%) and photocatalytic constant (k) for all the studied coatings

FIGURES

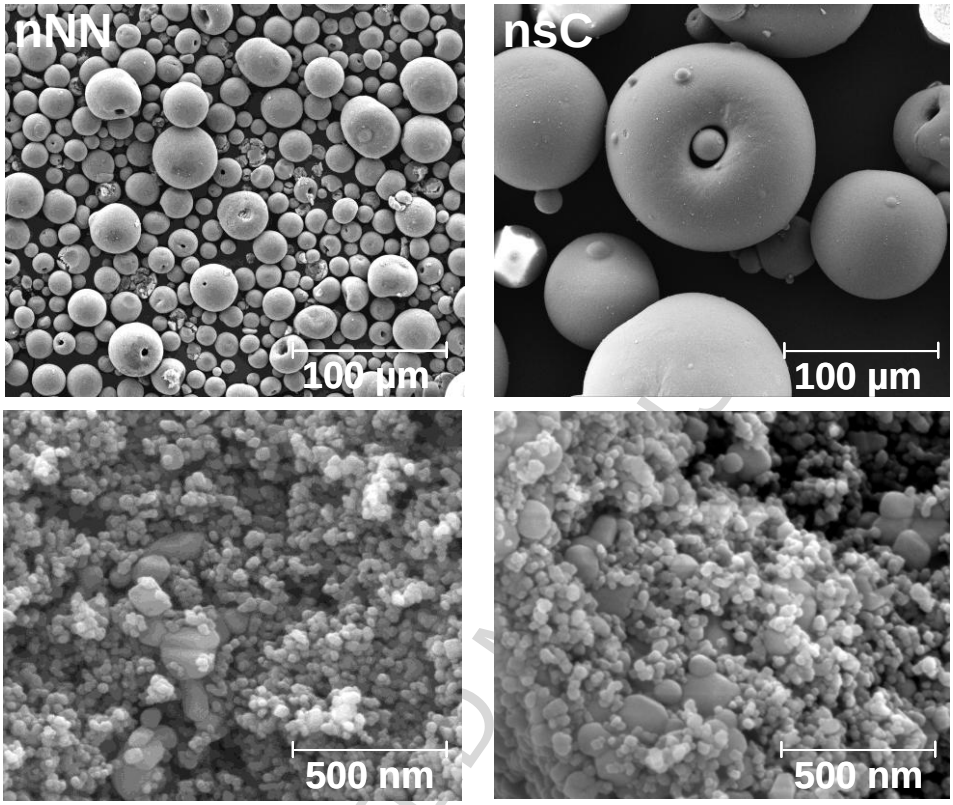

Figure 1

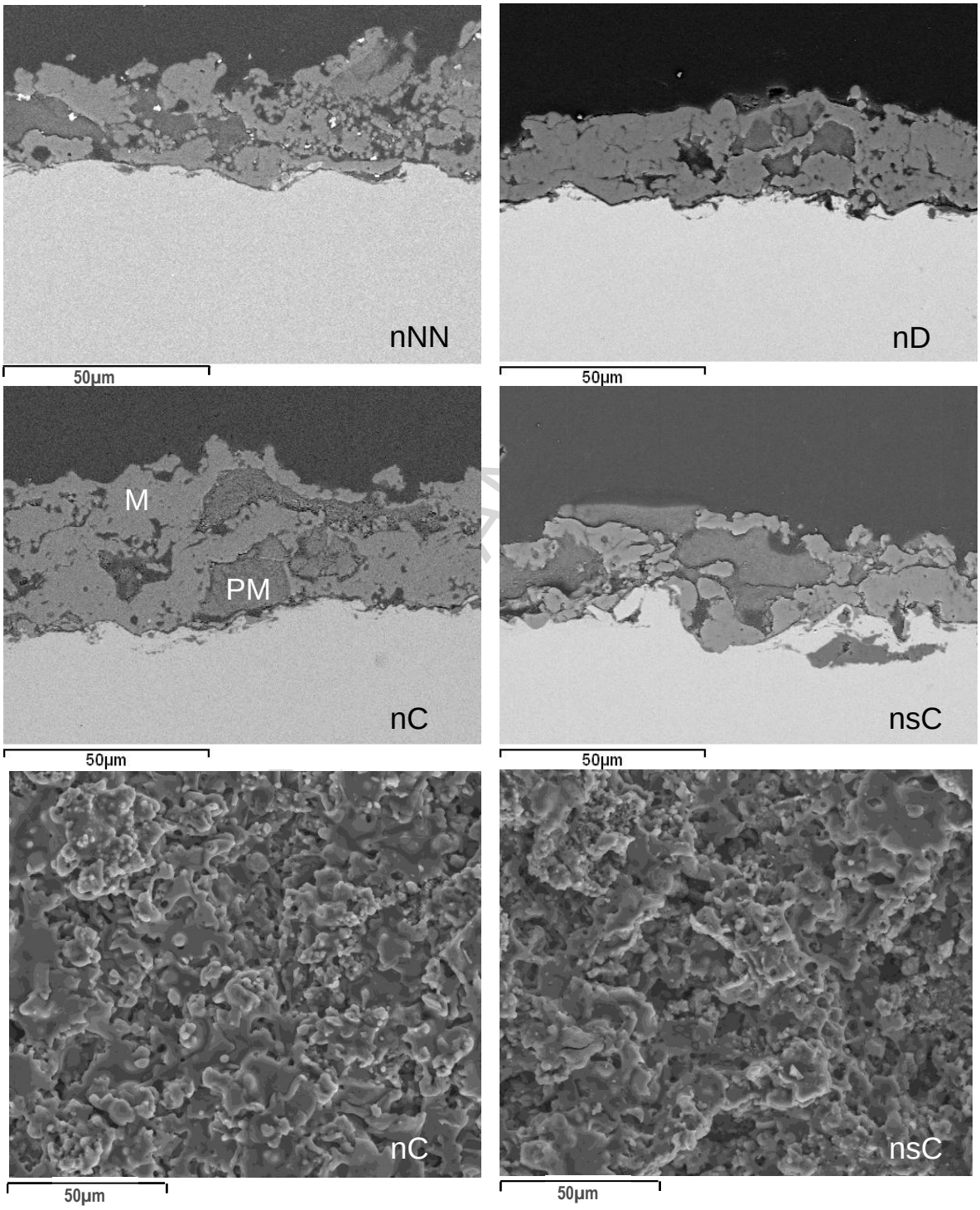

Figure 2

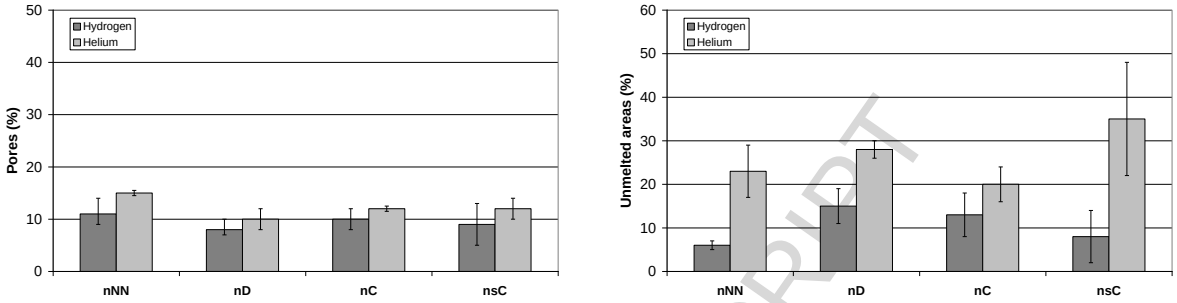

Figure 3

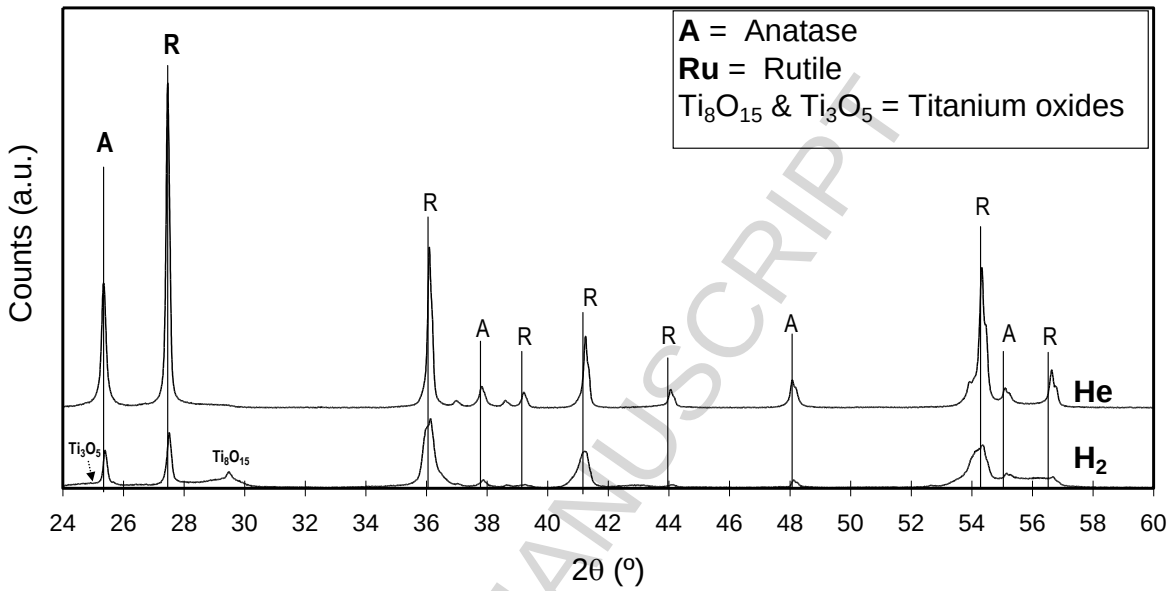

Figure 4

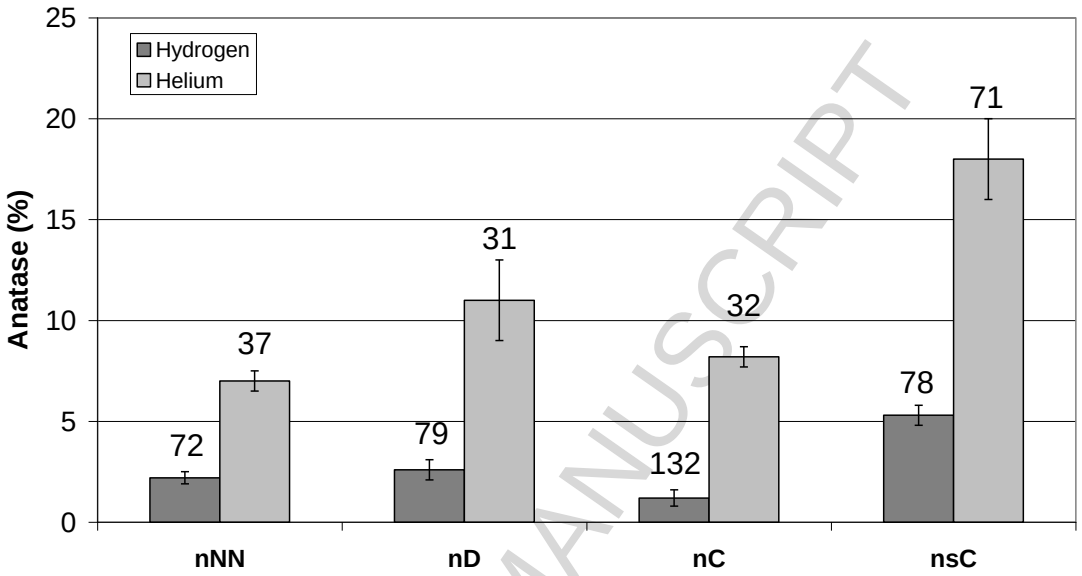

Figure 5

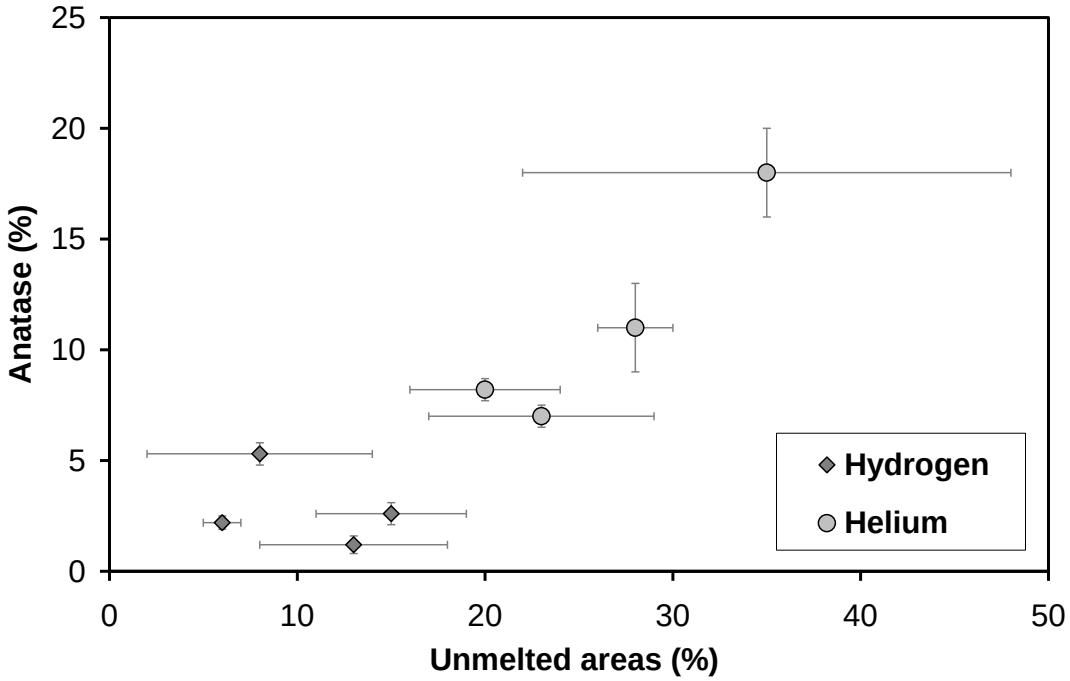

Figure 6

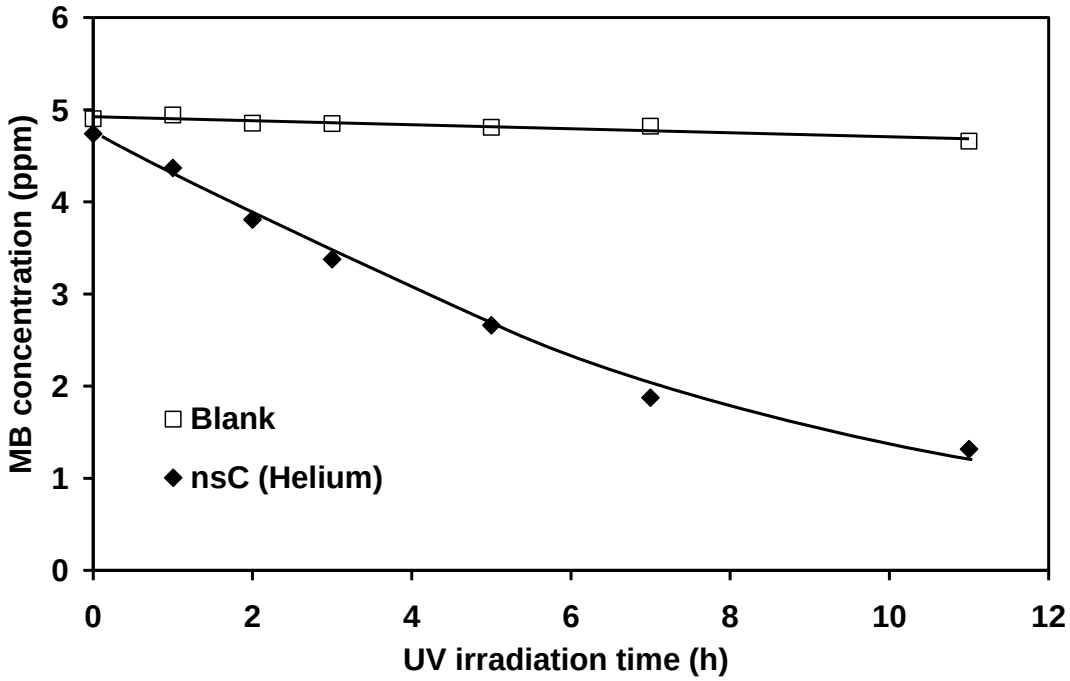

Figure 7

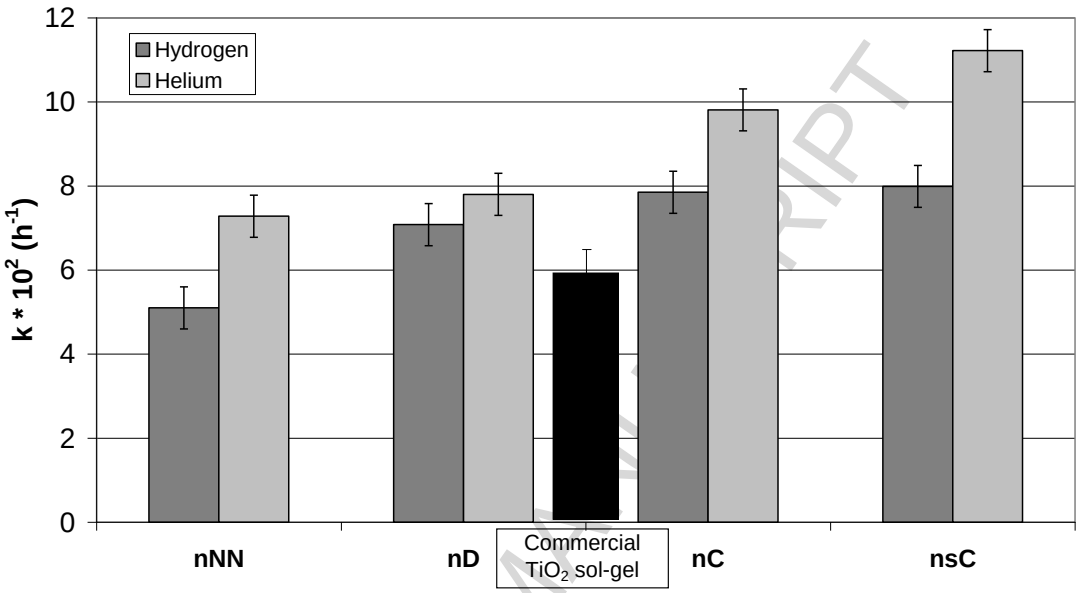

Figure 8

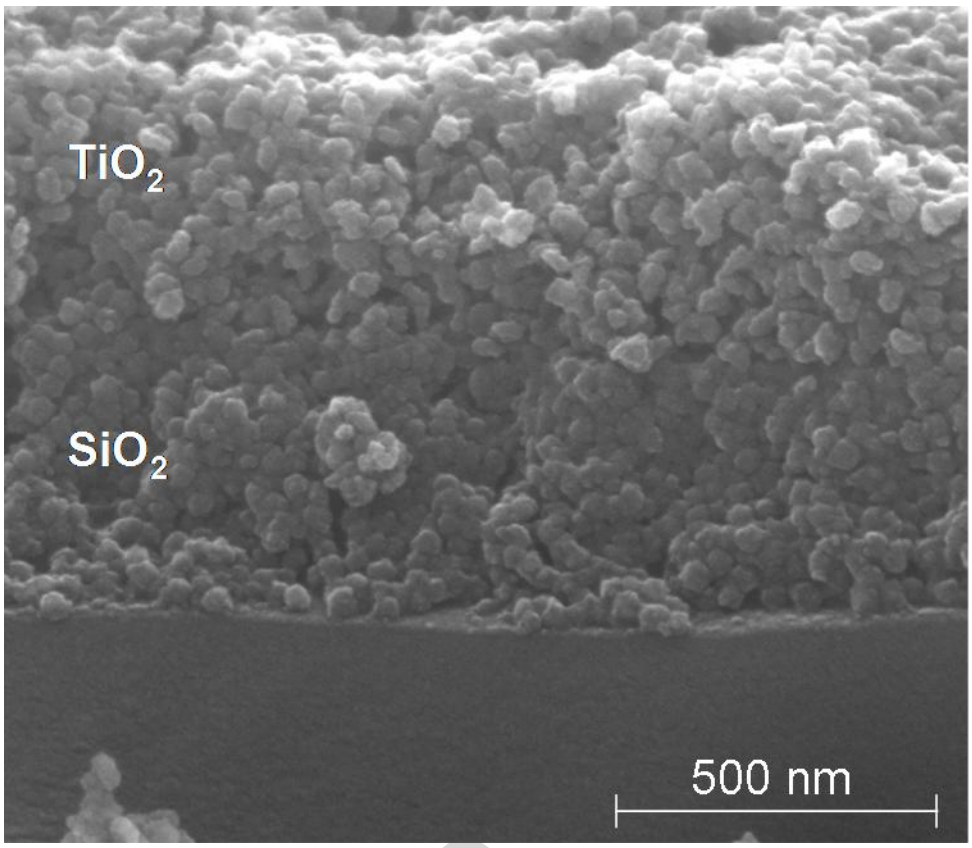

Figure 9

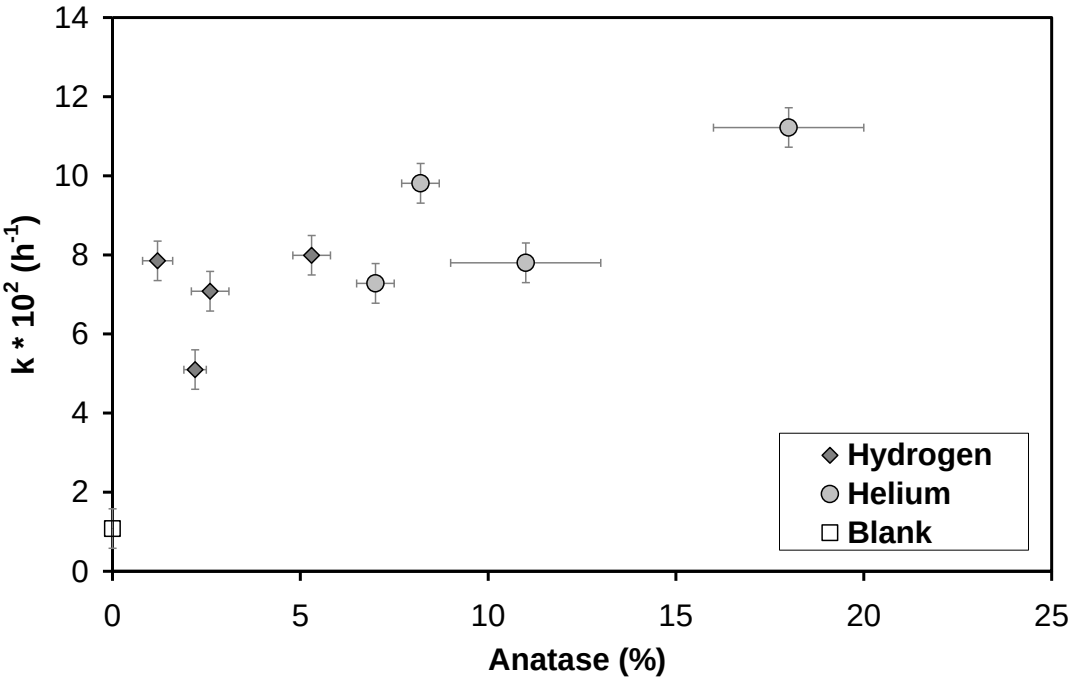

Figure 10

Highlights:

1. TiO_2 coatings were deposited by APS from 3 spray-dried powders.
2. XRD analysis revealed a mix of anatase and rutile in all coatings.
3. A bimodal microstructure was observed.
4. Anatase is mainly found in non-molten areas.
5. APS-coatings present better photocatalytic activity compared to commercial layer.